Available online at www.sciencedirect.com
ScienceDirect
Journal of Nuclear Materials 372 (2008) 141–151
journal of nuclear materials
www.elsevier.com/locate/jnucmat

Analysis of crack propagation in nuclear graphite using three-point bending of sandwiched specimens

Li Shi [a], Haiyan Li [a], Zhenmin Zou [a], Alex S.L. Fok [a,*], Barry J. Marsden [a], Andrew Hodgkins [b], Paul M. Mummery [b], James Marrow [b]

[a] School of Mechanical, Aerospace and Civil Engineering, The University of Manchester, P.O. Box 88, Sackville Street, Manchester M60 1QD, United Kingdom
[b] School of Materials, The University of Manchester, Grosvenor St., Manchester M1 7HS, United Kingdom

Received 4 October 2006; accepted 27 February 2007

Abstract

The aim of this paper was to assess the suitability of the sandwiched beam in three-point bending as a technique for determining fracture toughness and R-curve behaviour of nuclear graphite using small beam specimens. Surface displacements of the cracked beam specimen were measured using Electronic Speckle Pattern Interferometry (ESPI) and Image Correlation in order to accurately monitor crack propagation and frictional contact between the test specimen and the sandwiching beams. The results confirmed that solutions based on the simple beam theory could overestimate the fracture toughness of graphite. Finite element analysis using a Continuum Damage Mechanics failure model indicated that both friction and shape of the notch played an important part in providing resistance to crack growth. Inclusion of these factors and the use of more accurate load vs. crack length curves derived from the FE model would provide a satisfactory measure of fracture toughness in small beam specimens under such a loading configuration. The particular graphite tested, IG-110, showed a decrease in fracture toughness with increasing crack length.

1. Introduction

Graphite is used for the construction of structural components as well as neutron moderators in nuclear reactors. As graphite is a brittle material, cracking of these components can occur under the influence of thermal and mechanical stresses, especially those in relation to the dimensional and property changes induced by irradiation. The potential for using fracture mechanics to assess the structural integrity of nuclear graphite components has therefore become increasingly important and many attempts have been made to measure the fracture toughness of graphite [1–4,6].

Strictly speaking, standard methods of fracture toughness measurement only apply to homogeneous specimens containing a sharp crack, which in metals is typically produced by fatigue crack propagation from a machined notch. Crack branching often occurs when attempts are made to fatigue a sharp crack into brittle materials which have an inhomogeneous structure. Because of this difficulty, no standard fracture toughness test for brittle materials such as graphite has been established yet.

The first attempt to apply fracture mechanics principles to the fracture of nuclear graphite was probably that due to Corum [1]. He performed notched beam bend tests on an extruded graphite, used for the Experimental Gas-Cooled Reactor (EGCR), and evaluated the critical strain energy release rates based on linear elastic fracture mechanics. Calcined Continental-Lake Charles petroleum coke was used for this graphite, with a coal-tar pitch as the binder. The coke had needle-type particles, with a maximum particle size of ~0.8 mm. A typical beam specimen was 305 mm long, 31.7 mm wide and 31.7 mm deep. Notches of different depths were placed in the specimens using a 0.24 mm thick

* Corresponding author.
E-mail address: alex.fok@manchester.ac.uk (A.S.L. Fok).

0022-3115/$ - see front matter © 2007 Elsevier B.V. All rights reserved.
doi:10.1016/j.jnucmat.2007.02.012

jeweller's saw. Both the compliance measurement method and an analytical solution for the stress intensity factor were used to calculate the mode-I critical strain energy release rates (G_{IC}), and the two sets of results were reported to be in good agreement. However, there were uncertainties in measuring the compliance due to the nonlinear stress–strain behaviour of the graphite. G_{IC} values of about 70 and 50 J/m^2 for specimens whose axes are parallel and transverse to the direction of extrusion, respectively, were reported. The propagation of cracks was reported to be predominantly inter-granular. Lower G_{IC} values were observed for notch length-to-beam depth ratios (a/W) less than 0.2, for which the attributed causes included the occurrence of slow crack growth prior to unstable crack propagation, a sizable zone of inelastic deformation at the notch tip or pre-existing cracks or flaws. For example, if the shorter notches were assumed to have effective lengths equal to one or two maximum grain sizes (equivalent to the particle size) larger than the initial saw cut, the G_{IC} values recalculated with the adjusted lengths were roughly constant for all notch lengths.

Rose [2] measured the fracture toughness of virgin pitch coke graphite using curved notched beams cut from sleeves and subjected to bending. All tests were such that the direction of stressing was perpendicular to the extrusion direction of the graphite components. The notches had a root radius of about 0.5 mm and depth of 0.5–7.9 mm, giving notch depth to beam depth ratios between 0.03 and 0.52. By measuring acoustic emission, he demonstrated that micro-cracking took place prior to the main failure, with the quantity of micro-cracking decreasing with increasing notch depth. A modified solution based on Linear Elastic Fracture Mechanics (LEFM) was used to estimate K_{IC}. Similar to Corum [1], Rose found that consistent values of K_{IC} (1.2 MPa m$^{1/2}$) were obtained using the analytical method if an additional crack length of 0.6 mm was added to the original notch depth to account for the presence of inherent flaws. This applied also to unnotched specimens. However, the results from the compliance method to obtain the critical strain energy release rate showed a decrease in the measured fracture toughness with increasing notch depth.

Sakai et al. [3] used the compact tensile test with a chevron notch under loading and unloading to determine nonlinear elastic–plastic fracture parameters for an isotropic fine grain size polycrystalline graphite, IG-11, produced by Toyo Tanso Co. Ltd., Japan. These included the nonlinear critical strain energy release rate, the crack growth resistance, the J integral and the plastic energy dissipation rate. They found that about 38% of the total fracture energy was consumed as plastic energy. All of the fracture parameters decreased with increasing crack length for crack length to specimen width ratios (a/W) between 0.6 and 0.9. For zero plastic energy dissipation, i.e. as the crack length approaches the specimen width, the other three fracture parameters converge to give a lower limit of 73 J/m^2, which equates to a fracture toughness of 0.95 MPa m$^{1/2}$ for Young's modulus of 9.8 GPa and Poisson's ratio of 0.2.

In a separate paper [4], Sakai et al. examined the R-curve or crack growth resistance behaviour of another fine-grain polycrystalline graphite, IG-110, using the compact tensile test, ASTM E399 [5], with different notch depths ($0.3 < a/W < 0.9$). They showed that the R-curves rose sharply at first, then reached a plateau before falling off gradually for a/W ratios > 0.6. The initial sharp rise of the R-curves was attributed to grain bridging of the crack surfaces behind the primary crack tip, which had an initial root radius less than 10 μm, much smaller than those used in the other works mentioned. The final fall was attributed to the diminishing of material to sustain the micro-cracking process zone in front of the crack tip as the latter approaches the end face of the specimen. Note that the range of a/W values over which the R-curves fell off was the same as that for the IG-11 graphite mentioned above. The fracture toughness for stable crack propagation within the plateau region for this graphite was found to be 1.2 MPa m$^{1/2}$. Similar R-curve behaviour was found by Ouagne et al. [6] for PGA and IM1-24 graphites which are used as moderators in British Magnox and AGR nuclear reactors, respectively.

IG-110 was also investigated by Fazluddin using notched beams in three-point bend tests [7]. The crack lengths were monitored using the compliance method. Fig. 1 shows the resulting K_R curve reported in [7]. As can be seen from the figure, the K_R value of IG-110 changes very little over the range of crack lengths ($0.35 < a/W < 0.9$) examined, which is in contrast to the results reported by Sakai et al. [4] for this graphite using the compact tensile test.

From the above discussion, it is clear that the fracture toughness of graphite is ~1 MPa m$^{1/2}$, with $K_R \sim K_{IC}$, but the actual value measured seems to be sensitive to the test configuration, notch depth to specimen depth ratio, the geometry of the notch tip as well as the method of analysis. Similar observations on the same graphite have been made by Burchell et al. [8] who compared data from six different test geometries.

The sandwich beam bend test has been proposed by Pancheri et al. [9] as a method for pre-cracking brittle specimens since it is capable of producing sharp cracks with a certain length in a controlled manner. In this method, a rectangular beam with a saw cut of the material being tested is put between two sandwiching steel beams; see Fig. 2. The sandwich is then loaded in three-point bending. As the load increases, the crack would start to extend and, as it does so, the stiffness of the cracked beam would decrease and loading would be shed to the two sandwiching steel beams. The propagating crack would then slow down and arrest unless further load is applied. The test was applied to two different types of alumina, one with and one without significant R-curve behaviour, i.e. increase in fracture toughness with crack length. Using toughness data obtained from other tests, good agreement between theory

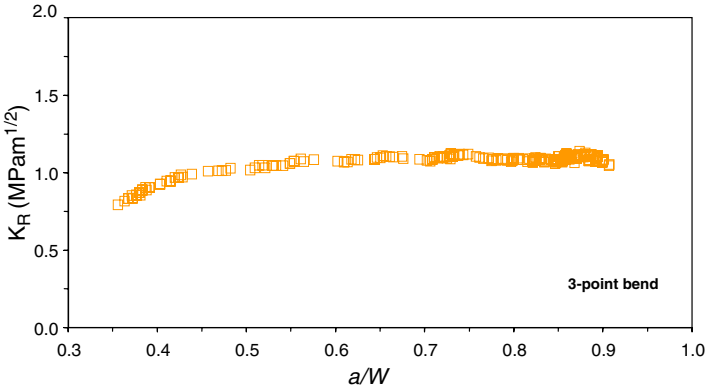

Fig. 1. K_R curve for IG-110 from three-point bend tests [7].

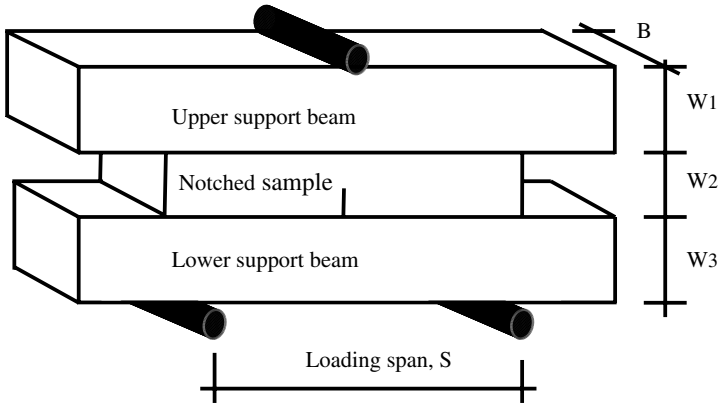

Fig. 2. Schematic of the sandwich beam bend test [8].

and experiments was reported in terms of the loads required to produce cracks of a certain length. Because of its simplicity, the authors went on to suggest the possibility of using such a test for measuring fracture toughness and R-curve behaviour directly.

The same test was used by Sglavo et al. [10] to pre-crack beam specimens of a wider range of brittle materials, including graphite. However, the apparent fracture toughness values based on simple beam theory were much higher than those measured subsequently by subjecting the pre-cracked beams, without sandwiching, to four-point bending. The authors attributed the discrepancy to friction between the beams and the initial finite notch root radius.

Despite these shortcomings, because it allows the use of a significantly smaller sample than the compact tension test, the sandwich beam bend test is of interest in the measurement of fracture toughness of neutron irradiated samples which are usually small and limited in numbers. The aims of this paper were (1) to apply the sandwich beam bend test to nuclear graphite, (2) to perform a more detailed assessment of the accuracy of the fracture toughness measured based on the stress intensity factor (SIF) solution proposed by Pancheri et al. [9], and (3) to derive more accurate load vs. crack length curves for fracture toughness measurements. Electronic Speckle Pattern Interferometry (ESPI) and Image Correlation techniques were used to measure the surface displacements of the cracked specimen as a means of monitoring accurately crack propagation. The fracture toughness of graphite thus measured was compared with data from existing literature. The discrepancy was then explained through the use of the finite element method, in conjunction with a Continuum Damage Mechanics (CDM) failure model, which examined quantitatively the effects of some of the factors ignored in the analytical solution provided by Pancheri et al. [9].

2. Analytical solution for the sandwiched specimen

Referring to Fig. 2, assuming that each beam deflects with the same curvature and ignoring frictional forces among the beams, the maximum bending moment, M_i, in the ith beam depends on its flexural stiffness, $(EI)_i$

$$M_i = M_{tot}\frac{(EI)_i}{(EI)_{tot}}, \tag{1}$$

where $M_{tot} = P_{tot}\, S/4$ and $(EI)_{tot} = \sum_i (EI)_i$, with S being the loading span and P_{tot} the total load applied to the sandwich.

The total load to be applied to the sandwich in order to obtain a crack to beam depth ratio a/W in a material with fracture toughness K_{IC} can then be expressed as

$$P_C = \frac{BW^{3/2}}{S}\frac{K_{IC}}{f(a/W)\Phi(a/W)}, \quad (2)$$

where B is the width of the specimen, W the depth and a the crack length. The function $f(a/W)$ was reported by Srawley [11] for the case $S = 4W$ as

$$f(\alpha) = 3\sqrt{\alpha}\frac{[1.99 - \alpha(1-\alpha)(2.15–3.93\alpha + 2.7\alpha^2)]}{2(1+2\alpha)(1-\alpha)^{3/2}}, \quad (3)$$

where $\alpha = a/W$. The non-dimensional function $\Phi(a/W)$ is defined as

$$\Phi(a/W) = \frac{(EI)_{sample}}{(EI)_{tot}} = \frac{1}{1 + (EI)_{beams}/(EI)_{sample}}, \quad (4)$$

where $(EI)_{beams}$ is the sum of the flexural stiffness of the sandwiching steel beams, $(EI)_{sample}$ is the flexural stiffness of the cracked sample and $(EI)_{tot} = (EI)_{beam} + (EI)_{sample}$. $(EI)_{sample}$ depends on the crack length, i.e. on the ratio a/W, and it can be expressed as [9]

$$\frac{(EI)_{sample}}{(EI)^0_{sample}} = (1-\alpha)^{3/2}(0.992 + 1.639\alpha - 6.225\alpha^2 + 7.063\alpha^3 - 3.324\alpha^4), \quad (5)$$

where $(EI)^0_{sample}$ is the flexural stiffness evaluated at $a/W = 0$, i.e. with no crack.

Curves of load versus the relative crack length a/W for different K_{IC} values can be obtained using Eq. (2); see for example Fig. 5.

3. Experimental work

The sandwich beam bend test was applied to the fine grain size (20 μm) nuclear graphite IG-110 to investigate the crack propagation behaviour of the material under such a loading configuration. The specimen used in the experiment is shown in Fig. 3. A rectangular graphite beam specimen was placed between two supporting steel beams, with the beams being able to slide freely against each other. A V-shape notch of depth a (2 mm) and root radius r (≈0.2 mm) was machined into the graphite sample. The use of a V-notch instead of one with vertical sides was justified by Rose who reported no difference in failure loads between the two types of notches of the same depth and root radius [2]. However, this would be shown to be untrue in a sandwich configuration; see later. The dimensions of the test configuration are $B_2 = 5$ mm, $a = 1$ mm, $W_2 = 5$ mm, $S = 20$ mm, $W_1 = W_3 = 2.5$ mm and $B_1 = 5.75$ mm. This sandwich was loaded in three-point bending as shown in Fig. 3.

As the stiffness of the steel beams was much larger than that of the graphite sample, the displacement of the sandwich was controlled by the support beams and increased very slowly with increasing applied load. Stable crack propagation was observed. This allowed optical imaging of the crack path and the crack tip process zone. Direct measurement of the specimen displacements was made using Electronic Speckle Pattern Interferometry (ESPI) and Image Correlation [12], from which strain fields could be calculated. Image correlation can be used to detect the crack tip position, whereas the more sensitive technique of ESPI, by recording a series of speckle patterns as the sample is loaded, is capable of building up a two-dimensional strain contour map of the surface. For example, the strain distributions obtained using image correlation as the crack propagated are shown in Fig. 4. The crack tip position is clearly identifiable.

The loads required to achieve stable cracks of different a/W ratios were calculated for K_{IC} values of 2.0 MPa $m^{1/2}$, 1.5 MPa $m^{1/2}$, 1.0 MPa $m^{1/2}$ and 0.5 MPa $m^{1/2}$ using

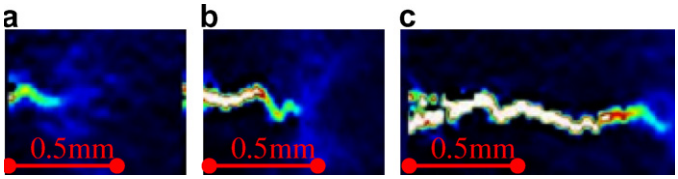

Fig. 4. Illustration of the increase in crack length and strain distribution, observed by image correlation under increasing load.

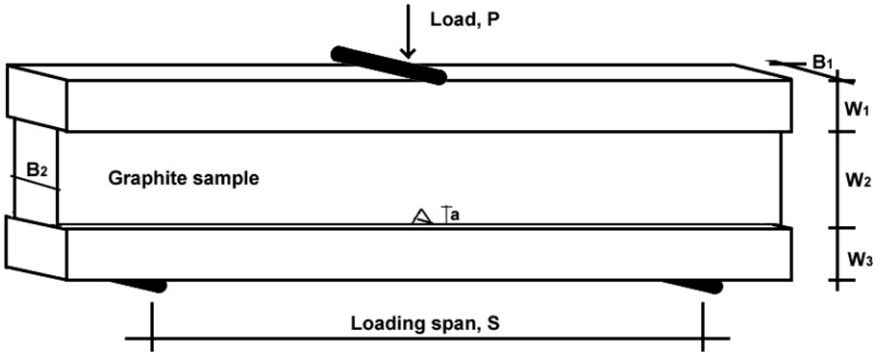

Fig. 3. Schematic of the specimen used in experimental work.

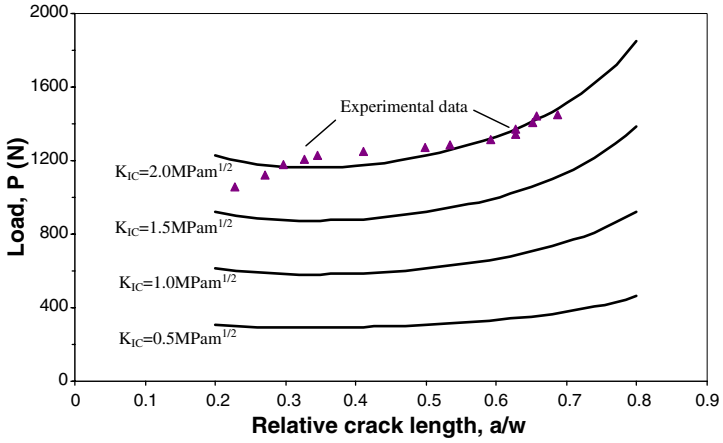

Fig. 5. Comparison between theoretical predictions and experimental data for load versus crack length.

Eq. (2). These were then compared with the experimental data, as shown in Fig. 5.

According to Fig. 5, IG-110 seems to exhibit typical R-curve behaviour with K_R showing an initial increase in value with increasing crack lengths before reaching a stable value. There is, however, no apparent decrease in K_R value with long crack lengths. Fig. 5 indicates a fracture toughness of 2.0 MPa m$^{1/2}$ for a/W values above 0.3. This is much higher than the values of 1.0–1.2 MPa m$^{1/2}$ reported in Refs. [4,7]; see also Fig. 2. Similar over estimations of fracture toughness have been reported by Sglavo et al. [10] who used the sandwich beam bend test to pre-crack specimens of a range of brittle materials, including graphite.

As pointed out by Pancheri et al. [9] and later by Sglavo et al. [10], the analytical solution used to construct the load versus crack extension curves contains some simplifications, which may lead to an overestimate of the crack tip stress intensity factor and hence the fracture toughness. First, friction at the boundaries between the steel beams and the specimen is expected to have a significant effect on the results of these tests. Second, the initial notch tip is not geometrically sharp. Third, the stresses experienced by the sandwiched specimen may be rather different from those of a standalone beam under three-point bending.

To address the first of these issues and to provide data on the friction coefficient for subsequent numerical analysis, bigger samples (Fig. 6) of a medium-grain graphite, Gilsocarbon, were loaded continuously, at a rate of 0.05 mm/min, until crack initiation occurred. ESPI was used to measure the displacements in the graphite and the steel sandwiching beams with increasing load (Fig. 7). The strain contour maps are obtained by differentiation of the displacements, averaged within a small sampling box of the order of 25 μm. Shear strains in the graphite and steel close to the interface are observed. These are illustrated in Fig. 8, which shows the strains immediately prior to the onset of sliding. The strains in the steel are clearly lower than the strains in the graphite. There was no significant strain measured in the vertical direction in either steel or graphite.

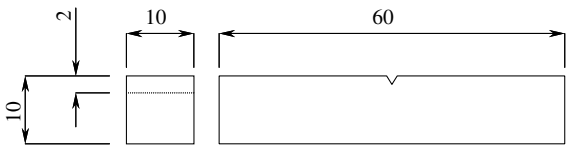

Fig. 6. Dimensions of the SENB specimen used to measure friction coefficient. All dimensions are in mm.

Fig. 9 shows the calculated static friction coefficient at the interface as a function of load. Slipping was detected, using ESPI, above a load of approximately 400 N. The friction co-efficient was estimated to be around 0.09–0.11, which is close to the values reported in the literature [13].

To assess the effects of friction between the beams and the discrepancy between the actual bending moment experienced by the specimen and that assumed in the analytical solution on the estimated fracture toughness, a detailed investigation using finite element (FE) analysis was undertaken.

A continuum damage mechanics (CDM) failure model for nuclear graphite has recently been developed and implemented into the commercial FE software, ABAQUS, in the form of interface elements [14]. In this model, both stress-based and fracture-mechanics-based failure criteria are used to construct a damage surface. The stiffness of the interface element is controlled by a damage factor (ω) which is a function of the interfacial displacements. The model can predict both the initiation and propagation of cracks in brittle components under mechanical loading. Fig. 10 shows schematically the creation of crack surfaces following material damage and the corresponding traction–displacement curve applied to the interface elements. A more detailed description of the model can be found in Refs. [14,15].

Much work has been carried out to verify the CDM model's accuracy and the results have indicated that the

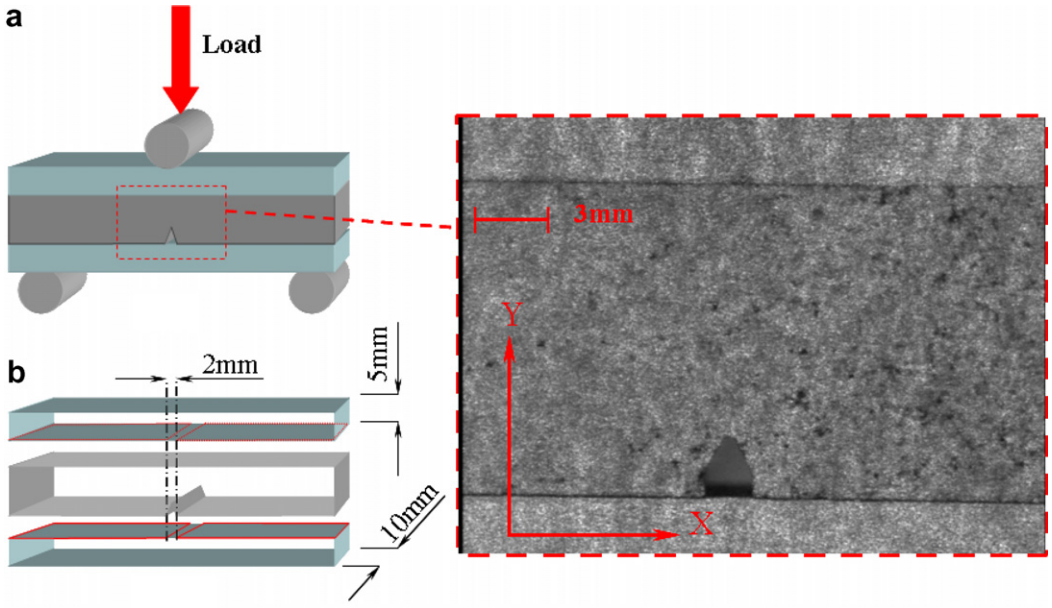

Fig. 7. Sandwiched SENB specimen (On the right is the region from the centre where ESPI was used to determine the static friction co-efficient (a). The area over which the load was distributed is highlighted in red in (b)). (For interpretation of the references in colour in this figure legend, the reader is referred to the web version of this article.)

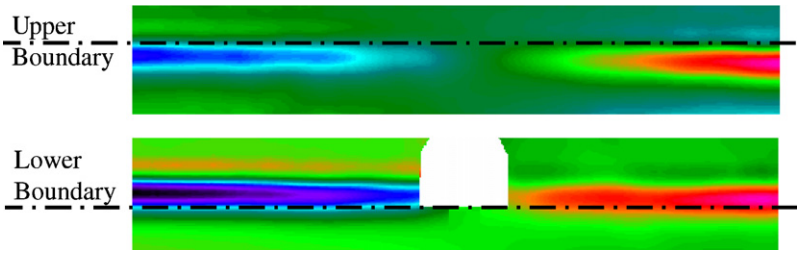

Fig. 8. Measured shear strain at the boundary between the specimen and the two sandwiching beams.

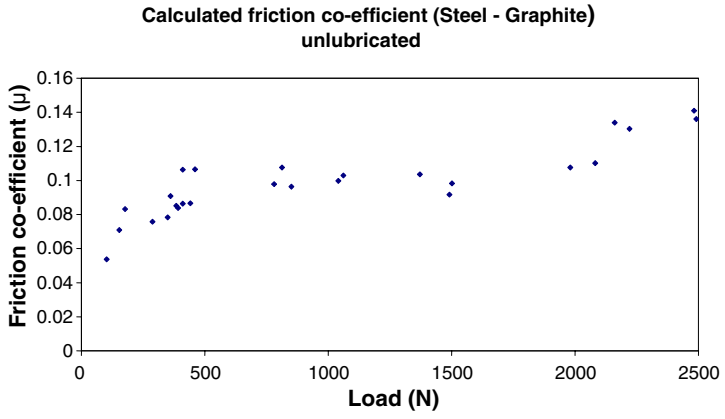

Fig. 9. Static friction co-efficient determined using strain contour maps from ESPI.

model is appropriate for fracture analysis of brittle materials [14–16]. In the present paper, crack propagation in the sandwiched beam under bend test is simulated using the CDM model and the results are used to provide more accurate load vs. crack length curves for fracture toughness measurement.

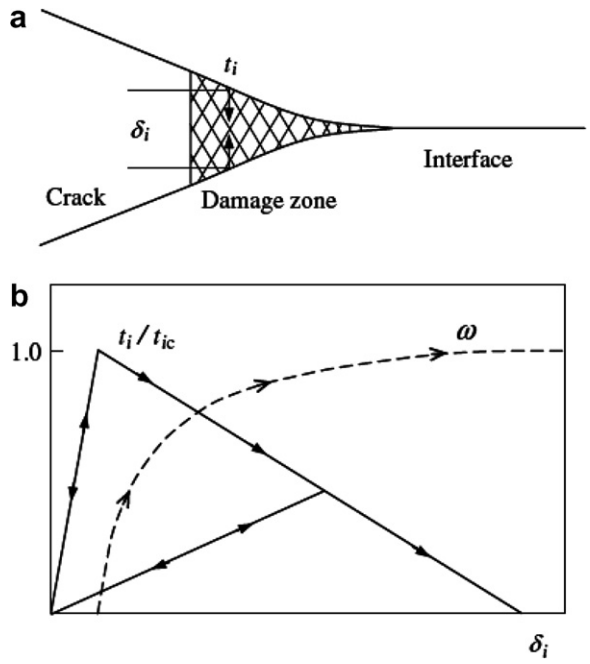

Fig. 10. (a) Interface, damage zone and fully formed crack (b) Interfacial traction (t_i)-displacement (δ_i) curve and damage evolution curve.

4. Finite element simulation for sandwiched specimen with a slit

A finite element analysis with 2 D quadrilateral plane-strain elements was first carried out for the same geometry as that adopted in [9], i.e. with a slit in the graphite beam. The corresponding finite element mesh is shown in Fig. 11.

Frictional contact was defined at the interfaces between the beams, with the coefficient of friction set at the measured value of 0.1. The displacements in the vertical direction at the support points a and b were restricted, and a prescribed displacement was applied at point c at the midsection. To capture the stress concentration in the vicinity of the crack tip, the mesh around the crack path was made much finer than that in the main region. In the present work, the crack was assumed to propagate along a predefined path AA in the middle (Fig. 11). There were dual coincident nodes along this assumed crack path for the introduction of interface elements to simulate the fracture process. Models with different numbers of interface elements along the assumed crack path were analysed and the results were compared with each other. It was found that 40 or more interface elements would provide a converged failure load. The final model used 50 interface elements.

In the CDM model, the properties of the graphite material were assumed to be [17]

$$E = 10.0\ \text{GPa}, \quad v = 0.2, \quad t_{1C} = 25\ \text{MPa}, \tag{6}$$

where E is Young's modulus, v is Poisson's ratio and t_{1C} is the tensile strength. Further, it was assumed that the shear strength has the same value as the tensile strength, i.e. $t_{1C} = t_{2C}$, but since the crack propagation in this case was mainly that of mode-I, the choice of shear strength was expected to have a negligible effect on the results. The critical strain energy release rate G_{IC} is related to the fracture toughness via

$$G_{IC} = K_{IC}^2(1 - v^2)/E. \tag{7}$$

Different fracture toughness values can be defined by changing the critical strain energy release rate G_{IC}. In the present analysis, models with K_{IC} equal to 1.5 MPa $m^{1/2}$, 1.0 MPa $m^{1/2}$ and 0.5 MPa $m^{1/2}$ were simulated. These have equivalent G_{IC} values of 216, 96 and 24 J m^{-2}, respectively. Similar to the fracture strengths, it was assumed that the fracture toughness for mode-I and mode-II were the same, i.e. $G_{IC} = G_{IIC}$.

The prescribed displacement (see Fig. 11) was increased from 0 to 0.15 mm in a step-by-step manner, using about 200 increments. At every increment, the reaction force at the loading point and the extent of damage of each interface element was recorded. When the damage factor ω, a measure of the percentage of micro-cracking, reached 1.0, the damaged interface element would be fully opened and become part of the extending crack. The predicted crack length was simply obtained from the total number of fully damaged elements.

The results prior to the onset of crack propagation were examined first to investigate the actual bending moment in the midsection of each beam and the frictional forces between the contact surfaces.

As can be seen from Fig. 12, the stress distribution of the graphite specimen in the sandwich configuration (the steel beams are not shown for clarity) is very different from that of the standalone beam under three-point bending, which was assumed for the theoretical calculation of the stress

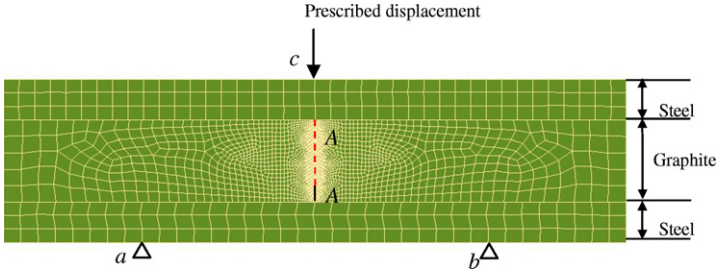

Fig. 11. FE mesh for sandwiched beam with a slit.

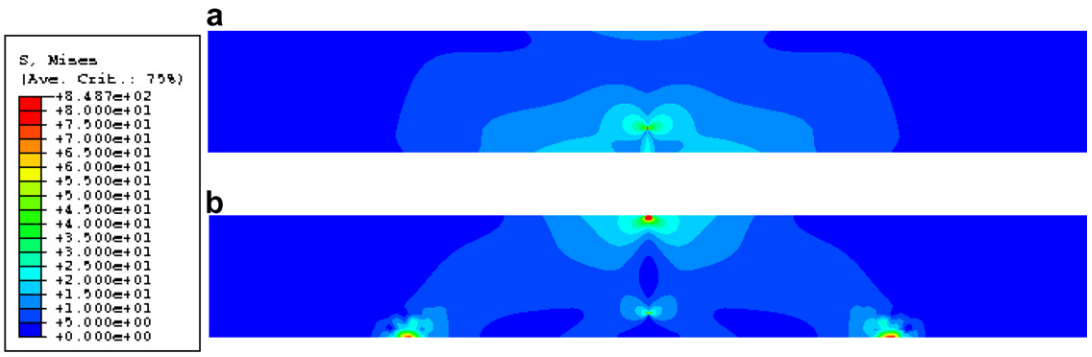

Fig. 12. Stress (σ_{xx}) contours of graphite beams under three-point bending: (a) sandwich configuration and (b) standalone (For clarity, the steel beams in (a) are not shown).

intensity factor. Loading in the sandwich configuration is more distributed; therefore, the bending moment produced is expected to be lower than that of a standalone beam.

Under a total load of 100 N, the frictional forces on the upper and lower contact surfaces of one half of the sandwiched graphite beam are calculated to be 5.0 N and 4.8 N respectively (see Fig. 13). Compared with the applied load, the frictional forces are significant and therefore cannot be ignored. The presence of the frictional forces will further affect the bending moment of each beam. In the

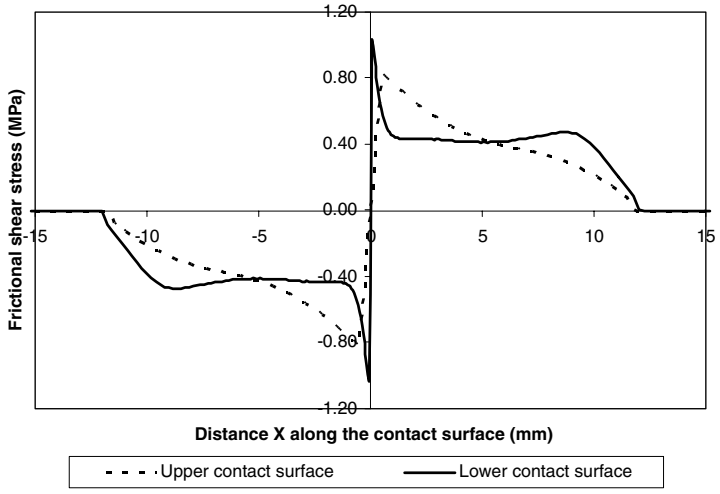

Fig. 13. Frictional forces on the top and bottom surfaces of the graphite beam.

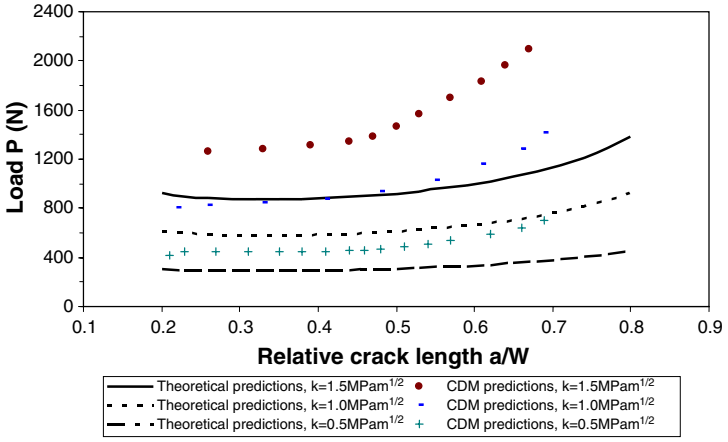

Fig. 14. Theoretical and FE predicted curves of load (P) versus relative crack length (a/W) for specimen with a slit.

theoretical analysis, the bending moment of each beam depends on their relative flexural stiffness only. According to Eq. (1), the bending moments of the upper steel beam, the graphite beam and the lower steel beam are 229.5 Nmm, 41.0 Nmm and 229.5 Nmm, respectively, for a load of 100 N. However, according to the FE analysis, the corresponding values are 208.8 Nmm, 26.2 Nmm and 228.5 Nmm, i.e. the analytical solution, by neglecting friction and the more distributed nature of loading, overestimates the bending moment for the graphite specimen by over 50%.

The above preliminary FE analysis indicates that the simplifications made in the analytical work may have led to an overestimate of K_{IC} for the IG-110 graphite tested. This justified the performance of more rigorous stress analysis using FE which could provide more accurate load vs. crack length curves for fracture toughness measurement.

The relationships between the applied load and the crack length for different fracture toughness values as predicted by the CDM model for the case with no friction are shown in Fig. 14, together with the analytical solutions. As can be seen, the FE model predicts higher load values for a given fracture toughness than the analytical solution, a clear indication that, when used to analyse the experimental data, the simple beam theory would overestimate the fracture toughness, even in the absence of friction. The difference is due to the load being more distributed in the sandwich configuration, as shown in Fig. 13.

5. Finite element simulation for sandwiched specimen with a V-notch

In the course of the numerical analysis, it was found that specimens with a slit behaved differently from those with a V-notch. The possible interaction between the cracked beam and the lower support beam through contact and friction could mean that a slit is more difficult to open up than a V-notch even though they behave similarly in a free beam, as observed by Rose [2]. This is supported by the results in Fig. 14 which shows that maximum shear forces occur immediately next to the slit. Therefore, to allow direct comparison between the experimental and FE results, the FE model was modified by replacing the slit with a V-notch in the graphite specimen. All the material properties and boundary conditions were the same as in the previous simulation. The analysis was carried out with and without friction between the graphite and steel. A typical plot showing the von Mises stress contours in the deformed beam with an opening crack is shown in Fig. 15.

Fig. 16 compares the FE predicted behaviour without friction with the experimental data. The results indicate a fracture toughness of 1–1.5 MPa $m^{1/2}$ for IG-110, with

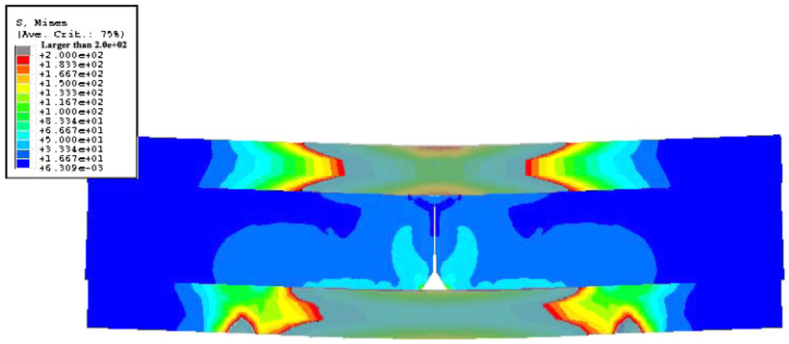

Fig. 15. Von-Mises stress contours and crack path from the FE analysis.

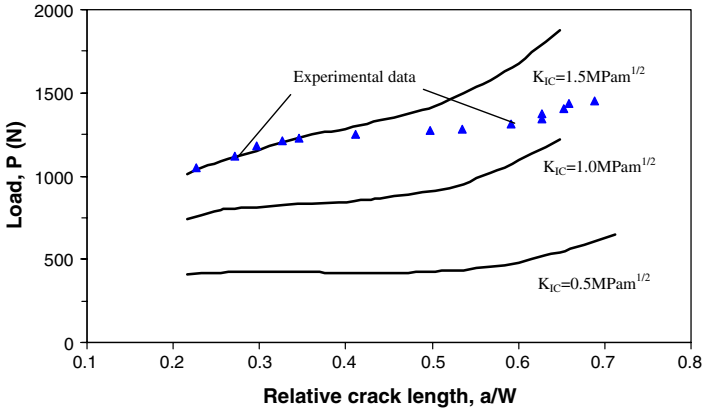

Fig. 16. Comparison between the Finite Element predictions (without friction) and experimental data for V-notched specimens.

the initial rise for short crack lengths no longer apparent and the toughness decreasing for crack lengths, a/W, greater than 0.4. These values are still higher than those reported elsewhere, pointing to the importance of friction in the analysis. Note that the curves in Fig. 16 are lower than those in Fig. 14, which were obtained for specimens with a slit. This confirms that, unlike a standalone beam, the shape of the notch, through its interaction with the support beam, can play an important part in providing resistance to crack growth.

Fig. 17 shows the FE predictions with an interfacial frictional coefficient of 0.1 between graphite and steel. The results now provide a fracture toughness which is much closer to existing data reported in the literature, i.e. a K_R value of 1.0 to 1.2 MPa $m^{1/2}$. Again, the predicted K_R values seemed to decrease as the crack approached the upper surface, but the a/W value at which this began was now higher at 0.5. According to Sakai et al. [4], this decrease in fracture toughness is due to the diminishing of material to sustain the damage process zone, which provides shielding to the crack tip, as the latter approaches the end face. The evolution of the damage process zone is schematically described in Fig. 18.

The ratio between the damage process zone size and the grain size is of great importance in the design of all mechanical tests for graphite. Fig. 17 indicates that the damage process zone size for IG-110, which has a mean grain size of 20 μm, is approximately half the beam depth, i.e. ~2.5 mm. On the other hand, using the relevant fracture parameters, it is estimated to be approximately 0.75 mm, or 0.15 of the beam depth. A possible explanation for this discrepancy lies in the fact that only part of the damage process zone was captured in the finite element model, since interface elements for modelling damage and fracture were placed along the midline of the notched beam only. Had the damage process zone been modelled more fully, the FE-predicted curves of $K_{IC} < 1.2$ MPa $m^{1/2}$ would be expected to become closer to the experimental data (Fig. 17), with the reduction in fracture toughness taking place at a higher a/W value. This means the results would be similar to those reported by Fazluddin [7] who tested IG-110 using single edge-notched beams in three-point bending and found no significant reduction in fracture toughness with increasing crack length (Fig. 1).

6. Conclusions

The sandwiched beam in three-point bending has been applied to IG-110 nuclear graphite to assess its suitability for determining fracture toughness and R-curve behaviour of brittle materials. This simple test configuration gave stable crack propagation, which allowed the use of optical imaging to accurately determine the length of the extending crack. However, finite element analysis using a continuum damage mechanics failure model shows that solutions based on simple beam theory would overestimate the fracture toughness of materials, especially when frictional forces among the beams are significant and need to be

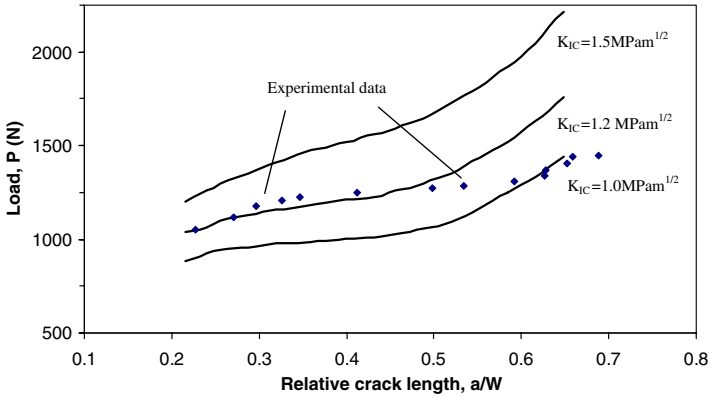

Fig. 17. Comparison between the Finite Element predictions (with friction) and experimental data for V-notched specimens.

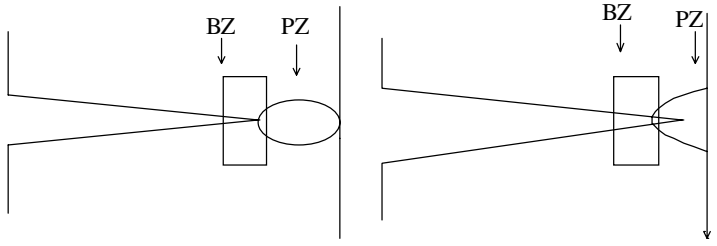

Fig. 18. Schematic showing evolution of the crack bridging (BZ) and damage process (PZ) zones.

considered in the calculation. Inclusion of these forces, which can be measured indirectly by observation of the specimen displacements, and the use of more accurate load vs. crack length curves derived from the FE model provides a satisfactory measure of fracture toughness and its dependence on the crack length in small beam specimens.

Acknowledgements

The financial support of the Health and Safety Executive through Contract No. NUC/56/60/5 is gratefully acknowledged. The views expressed in this paper are those of the authors and do not necessarily represent the views of the Health and Safety Commission/Executive.

References

[1] J.M. Corum, J. Nucl. Mater. 22 (1967) 41.
[2] A.P.G. Rose, Carbon 23 (4) (1985) 387.
[3] M. Sakai, K. Urashima, M. Inagaki, J. Am. Ceram. Soc. 66 (12) (1983) 868.
[4] M. Sakai, J. Yoshimura, Y. Goto, M. Inagaki, J. Am. Ceram. Soc. 71 (8) (1988) 609.
[5] ASTM Standard E399-81, Annual book of ASTM Standards, Part 10, ASTM, Philadelphia, PA, (1983).
[6] P. Ouagne, G.B. Neighbour, B. McEnaney, J. Phys. D: Appl. Phys. 35 (2002) 927.
[7] S. Fazluddin, Crack Growth Resistance in Nuclear Graphite, PhD thesis, Department of Materials, The University of Leeds, July (2002).
[8] T.D. Burchell, T. Oku and M. Eto. A Comparison of Fracture Toughness Measurement Techniques as Applied to Nuclear Graphite. In Ext. Abs. & Prog. Carbone 90, Paris, France. July 16–20 (1990) p. 278.
[9] P. Pancheri, P. Bosetti, R. Dal Maschio, V.M. Sglavo, Eng. Fract. Mech. 59 (4) (1998) 447.
[10] V.M. Sglavo, P. Bosetti, E. Trentini, M. Ceschini, J. Am. Ceram. Soc. 82 (8) (1999) 2269.
[11] J.E. Srawley, Int. J. Fract. 12 (1976) 475.
[12] D. Denby, J.A. Leendertz, J. Strain Anal. 9 (1) (1974) 17.
[13] J. Carvill, Mechanical Engineer's Data Handbook, Butterworth-Heinemann, 1994.
[14] Z. Zou, S.L. Fok, S.O. Oyadiji, B.J. Marsden, J. Nucl. Mater. 324 (2004) 116.
[15] Z. Zou, S.L. Fok, B.J. Marsden, S.O. Oyadiji, Eng. Fract. Mech. 73 (2006) 318.
[16] L. Shi, H. Li, S.L. Fok, B.J. Marsden, S. Yu, in: 2nd International Topical Meeting on High Temperature Reactor Technology, Beijing, China, September 22–24, 2004.
[17] K. Kikuchi, M. Futakawa, in: Specialists' meeting on graphite component structural design, JAERI Tokai (Japan), September 8–11, in: IAEA, International Working Group on Gas-Cooled Reactors IWGGCR – 11, 1986, p. 138.